

波浪诱导粉砂质海床中的瞬态孔压响应：相位滞后与幅值衰减

李畅飞^{1,2}, 高福平^{1,2*}

¹ (中国科学院力学研究所流固耦合系统力学重点实验室, 北京 100190) ² (中国科学院大学工程科学学院, 北京 100049)

摘要: 在波浪荷载作用下, 粉砂质海床内部会被诱导产生瞬态超静孔压。瞬态孔压响应表现为随波浪周期振荡的特性, 并伴随着相位滞后与幅值衰减。本文基于瞬态孔压响应的解析解, 分析了渗透系数和饱和度对相位滞后的影响; 通过水槽试验, 对波浪作用下砂土和粉土海床瞬态孔压响应的幅值与相位进行了观测, 并与多孔弹性介质海床瞬态孔压响应的解析解进行了对比。研究发现, 相位滞后主要由渗透系数与饱和度控制; 渗透系数越小, 饱和度越低, 相位滞后在海床表层的变化梯度越大。瞬态孔压响应的试验值与理论解具有良好的吻合度。砂土海床内部瞬态孔压的相位滞后与幅值衰减变化梯度较小, 相位滞后随海床深度的增加而单调增大; 粉土海床内部瞬态孔压的相位滞后与幅值衰减变化梯度较大, 并且相位滞后随海床深度呈先增大后减小的变化趋势。

关键词: 瞬态超静孔压, 相位滞后, 幅值衰减, 理论分析, 水槽试验

引言

在近海工程实践中, 波浪荷载将诱导海床内部产生超静孔隙水压力, 进而导致海床承载力降低, 甚至可能发生液化。由此引发的海洋结构失稳时有发生, 比如防波堤的倾倒^[1], 海底埋设管线的上浮^[2]等。波浪荷载诱导土体内部产生的超静孔压存在两种动态响应机制: 累积孔压响应和瞬态孔压响应^[3]。前者为海床土骨架剪缩趋势引起的孔隙水压增减效应, 与地震作用下土体液化类似^[4]; 而后者又称振荡孔压, 为超静孔隙水压力的实时脉动响应。

波浪诱导瞬态孔压响应的研究通常基于比奥固结理论^[5], 假定海床土体满足线弹性本构关系及达西定律。Putnam (1949)^[6]假定海床为刚性, 孔隙水不可压缩, 提出了有限深度、各向同性海床瞬态孔压响应的解析解。Moshagen & Torum (1975)^[7]考虑了孔隙水的可压缩性, 提出了各向同性海床瞬态孔压响应的解析解。Yamamoto et al. (1978)^[8]同时考虑了孔隙水以及海床土骨架的变形, 提出了无限深度、各向同性海床内部瞬态孔压响应、土骨架位移及有效应力的解析解。Madsen (1978)^[9]基于与 Yamamoto et al. (1978)相同的假设, 得到了无限深度、水力各向异性海床内部瞬态孔压和有效应力的一般解。Hsu & Jeng (1994)^[10]将理论解推广至有限深度海床, 当海床深度足够大时, 该理论解可以退化至 Yamamoto et al. (1978)和 Madsen (1978)提出的解析解。Mei & Foda (1981)^[11]假设排水过程仅发生在靠近海床表面的薄层, 提出了求解波浪荷载下海床内部瞬态响应的边界层理论。除了上述理论解, 关于海床瞬态响应的数值模拟^[12-16]和物理试验^[17-21]也得到了广泛开展。Jeng (2018)^[22]对波浪荷载下的海床响应模型作了系统的综述。

瞬态孔压响应通常伴随着相位滞后与幅值衰减^[8]。本文将基于 Yamamoto et al. (1978)提出的瞬态孔压响应解析解, 结合水槽试验, 分别对砂质海床与粉质海床内部的相位滞后与幅值衰减特征进行研究。进而推导低饱和度海床内部相位滞后的理论解, 并对影响相位滞后的关键控制参量进行分析。最后, 将理论解与水槽试验数据进行对比, 探究砂土与粉土海床瞬态孔压响应特性的异同。

1 相位滞后与幅值衰减: 理论分析

1.1 瞬态孔压响应解析解

Yamamoto et al. (1978)提出的波浪荷载下瞬态孔压响应解析解可以表示为:

$$p(z) = p_b [(1-\alpha) \exp(-\lambda z) + \alpha \exp(-\lambda' z)] \quad (1)$$

其中 $p_b = \frac{\gamma_w H}{2 \cosh \lambda d} \exp[i(\lambda x + \omega t)]$ 为床面波压力, $p_0 = \frac{\gamma_w H}{2 \cosh \lambda d}$ 为床面波压力幅值, H 为波高, $\lambda (=2\pi/L)$ 为波数, L 为波长, ω 为波浪圆频率, 记 $\theta = \lambda x + \omega t$ 为表面水波及床面波压力的脉动相位, d 为水深, $\alpha = \frac{im\omega''}{-\lambda'' + i(1+m)\omega''}$, $m = \frac{n}{K'} \frac{G}{1-2\nu}$, $(\lambda')^2 = \lambda^2 + i \frac{\gamma_w}{k_s} \omega \left(\frac{n}{K'} + \frac{1-2\nu}{2(1-\nu)G} \right)$, $\omega'' = \beta (\omega' / \lambda^2)$, $\beta = \frac{1-\nu}{1-2\nu}$, $\lambda'' = (\lambda' - \lambda)/\lambda$, $\omega' = \omega/c$, $c = \frac{k_s}{\gamma_w} / \left(\frac{n}{K'} + \frac{1-2\nu}{2(1-\nu)G} \right)$, i 为虚数单位, G 为剪切模量, n 为孔隙率, k_s 为渗透系数, ν 为泊松比, K' 为孔隙流体的体变模量, 经由下式计算:

$$\frac{1}{K'} = \frac{1}{K} + \frac{1-S_r}{P_0} \quad (2)$$

其中 $K(=1.9 \times 10^9 \text{ Pa})$ 为纯水的体变模量, S_r 为饱和度, P_0 为海床表面的绝对静水压力。研究表明, 饱和度对于孔隙流体的体变模量具有显著影响, 也是影响瞬态孔压响应的关键参量(Okusa, 1985^[23]; Sakai et al., 1992^[24])。图 1 给出了水深 $d=10\text{m}$ 情况下, 体变模量随饱和度的变化, 可以看出, 体变模量随饱和度的变化较为敏感。

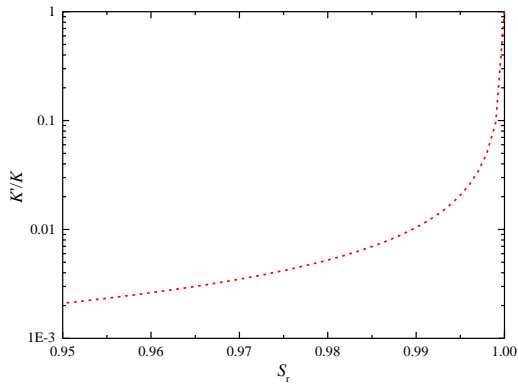


图 1 饱和度对孔隙流体体变模量的影响($d=10\text{m}$)

Fig. 1 Effects of degree of saturation on the apparent bulk modulus of pore-fluid ($d=10\text{m}$)

1.2 完全饱和与低饱和海床瞬态孔压响应特性

对于完全饱和海床, 其孔隙内部不含气体, 此时 $G/K' \rightarrow 0$, $m \rightarrow 0$, $\alpha \rightarrow 0$, (1)式可以化为:

$$p(z) = \frac{\gamma_w H}{2 \cosh \lambda d} \exp(-\lambda z) \exp[i(\lambda x + \omega t)] \quad (3)$$

可以看出, 此时瞬态孔压幅值呈指数型衰减, 衰减率为 $e^{-\lambda z}$, 波数越大, 孔压幅值衰减越显著; 浅层海床的瞬态孔压振荡幅值相较深层海床具有更大的衰减率。完全饱和海床内部瞬态孔压响应不会出现相位滞后, 其与床面波压力及表面水波具有相同的相位。

对于低饱和度海床, 其孔隙内部含有一定量气体, 致使土骨架的刚度远远大于孔隙流体的刚度, 此时 $G/K' \rightarrow \infty$, $m \rightarrow \infty$, $\alpha \rightarrow 1$, (1)式可以化为:

$$p(z) = \frac{\gamma_w H}{2 \cosh \lambda d} \exp(-\lambda' z) \exp[i(\lambda x + \omega t)] \quad (4)$$

且有

$$(\lambda'^2) = \lambda^2 + i \frac{\gamma_w}{k_s} \omega \left(\frac{n}{K'} + \frac{1-2\nu}{2(1-\nu)G} \right) \rightarrow \lambda^2 + i \frac{\omega \gamma_w}{k_s} \frac{n}{K'} \quad (5)$$

其中 λ' 为复数形式, 记 $\lambda' = a + bi$, a , b 均为实数, 将(5)式代入(4)式, 得到:

$$p(z) = \frac{\gamma_w H}{2 \cosh \lambda d} e^{-az} e^{i(\theta - bz)} \quad (6)$$

此时瞬态孔压幅值随海床深度呈指数型衰减, 衰减率为 e^{-az} ; 瞬态孔压响应出现相位滞后, 其大小

为 bz , 随海床深度线性增加。将 $\lambda' = a + bi$ 代入(5)式, 得到:

$$a^2 - b^2 = \lambda^2 \quad (7a)$$

$$2ab = \frac{n\omega\gamma_w}{K'k_s} \quad (7b)$$

考虑到 $a, b > 0$, 可以解得:

$$a = \left(\frac{\lambda^2 + \sqrt{\lambda^4 + (\frac{n\omega\gamma_w}{K'k_s})^2}}{2} \right)^{\frac{1}{2}} \quad (8a)$$

$$b = \left(\frac{-\lambda^2 + \sqrt{\lambda^4 + (\frac{n\omega\gamma_w}{K'k_s})^2}}{2} \right)^{\frac{1}{2}} \quad (8b)$$

由(8a)式, 可以看出 $a > \lambda$, 因而低饱和度的海床相较完全饱和海床孔压衰减率更快。由于 a, b 有同时增大亦或减小的变化趋势, 因而更大(小)的幅值衰减也意味着更大(小)的相位滞后。在给定波浪参数的情况下, 相位滞后的值仅与海床土体的孔隙率 n 、渗透系数 k_s 及孔隙流体的体变模量 K' 有关。

图 2 给出了在 $k_s K'$ 为定值的情况下, 瞬态孔压响应相位滞后随深度的变化。分析选取的波浪及土性参数分别为: $d=0.6m$, $T=1.5s$, $G=10MPa$, $n=0.35$, $\nu=0.25$ 。可以看出, 随着 G/K' 逐渐增大, 相位滞后的值越趋近于 bz ; 当 G/K' 达到 10^2 量级时, 相位滞后可由 bz 的值精确估算。

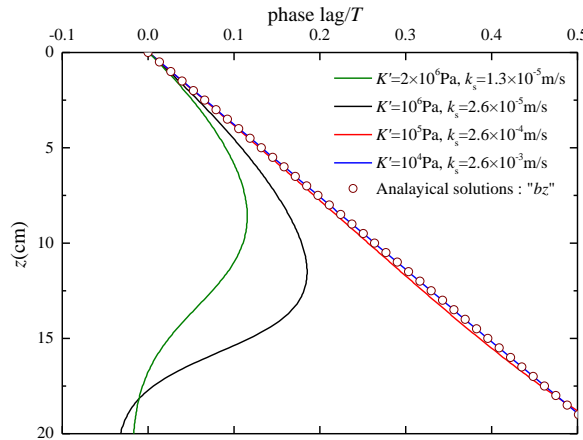


图 2 $k_s K'$ 为定值时相位滞后随海床深度的变化

Fig.2 Vertical distribution of the phase-lag of excess pore pressure when $k_s K'$ is constant

1.3 饱和度与渗透系数对相位滞后的影响

本节将基于参量分析, 研究海床饱和度(或孔隙流体的体变模量)以及渗透系数对相位滞后的影响。图 3 分别给出了高渗透性(取 $k_s \geq 10^{-4} m/s$)海床(如中砂, 粗砂等)和低渗透性(取 $k_s < 10^{-4} m/s$)海床(如细砂, 粉土等)相位滞后随深度的变化。计算选取的波浪及土性参数分别为: $d=0.6m$, $T=1.5s$, $G=10MPa$, $n=0.35$, $\nu=0.25$ 。鉴于瞬态孔压响应在深层海床较为微弱, 图 3 仅给出了较浅层海床($z < 20cm$)相位滞后的变化状况。可以看出, 对于渗透性良好的海床, 相位滞后呈现单调变化。渗透系数越小, 饱和度越低, 相位滞后越显著。对于渗透性较差的海床, 相位滞后呈现非单调变化, 相位差可能为负值。此时渗透系数越小, 饱和度越低, 表层海床相位滞后变化梯度越显著; 在深层海床, 相位滞后逐渐趋于零。

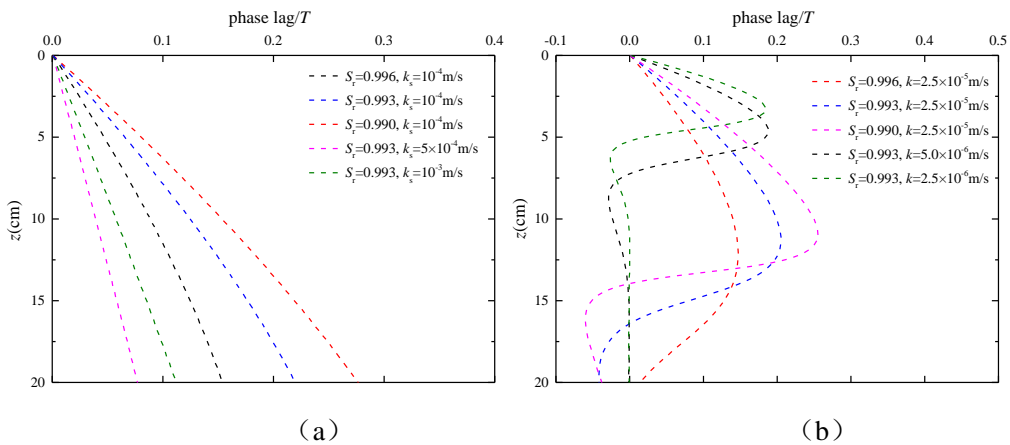


图 3 饱和度与渗透系数对相位滞后特性的影响: (a) 高渗透性海床 (b) 低渗透性海床
Fig. 3 Effects of degree of saturation and permeability on the phase-lag: (a) seabed with high permeability (b) seabed with low permeability

2 相位滞后与幅值衰减: 试验研究

2.1 波浪诱导砂土与粉土海床孔压响应

本文选取砂土海床和粉土海床在波浪荷载下的水槽响应试验对瞬态响应特性进行研究, 试验中海床土性参数及波浪荷载如表 1。

表 1 水槽试验中的波浪荷载及土性参数

Table 1. Soil properties and wave parameters in the flume experiment

Parameter	Symbol	Value	
		Sandy seabed	Silty seabed
Porosity of soil	n	0.44	0.35
Coefficient of permeability	k_s (m/s)	1.88×10^{-4}	2.6×10^{-6}
Soil properties	S_r	0.995	0.996
Shear modulus	G (MPa)	10	10
Poisson ratio of soil	ν	0.3	0.25
Water depth	d (m)	0.5	0.6
Wave parameters	T (s)	1.2	1.5
	H (cm)	9.5	8.0

图 4 分别给出了试验中的自由水面波动曲线 η 及海床不同深度处超静孔压 p 时程发展曲线。波浪荷载下的砂土海床内部仅存在瞬态孔压响应, 而粉土海床内部将出现累积孔压和塑性变形。因此, 本文将选取波浪加载初期粉土海床内部的超净孔压时程发展曲线, 以使粉土海床响应更接近于弹性响应。由图 4 可以看出, 瞬态孔压振荡幅值随深度呈现显著的衰减, 并伴随着相位滞后现象。

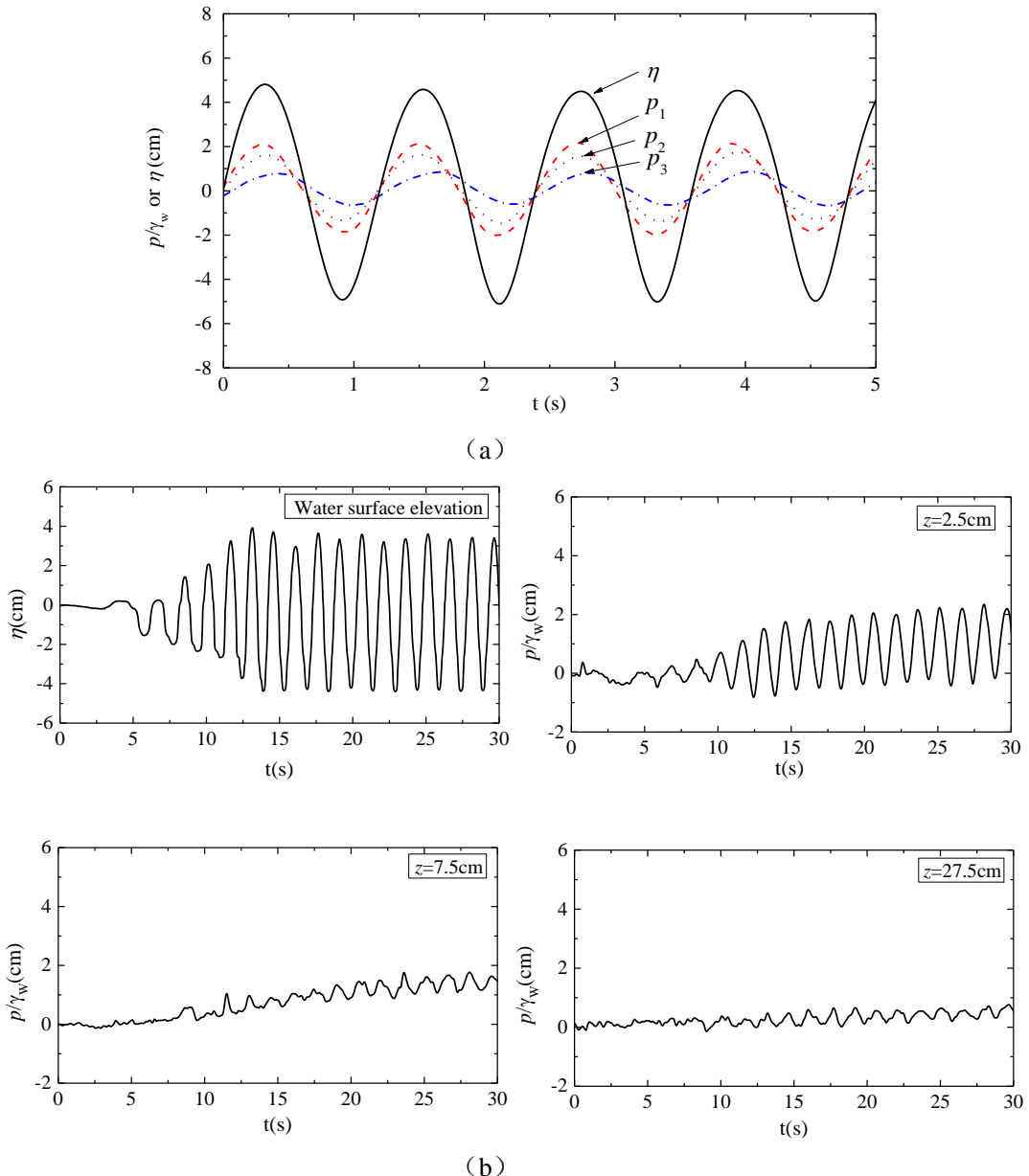


图4 表面水波及超静孔压时程曲线: (a) 砂土海床^[21] (b) 粉土海床

Fig. 4 Time series of the water surface elevation and wave induced pore pressure for different seabed depth: (a) sandy seabed ^[21](b) silty seabed

2.2 相位滞后与幅值衰减: 试验值与理论解对比

图5给出了两种海床瞬态孔压响应相位滞后与幅值衰减的试验值与理论解对比状况。可以看出, 经由多孔弹性理论预测的瞬态孔压响应特性与试验数据吻合良好。砂土海床幅值衰减较为缓慢, 相位滞后随深度单调增加; 粉土海床表层的幅值衰减更加剧烈, 相位滞后呈现非单调变化, 当超过某一临界深度 ($z_{cr} \approx 7.5\text{cm}$) 后, 孔压响应较为微弱并且几乎不随深度发生变化。粉土海床的瞬态响应特性与边界层类似, 在边界层内部, 相位滞后与幅值衰减具有较大的梯度, 与砂土海床的响应特性有显著的区别。

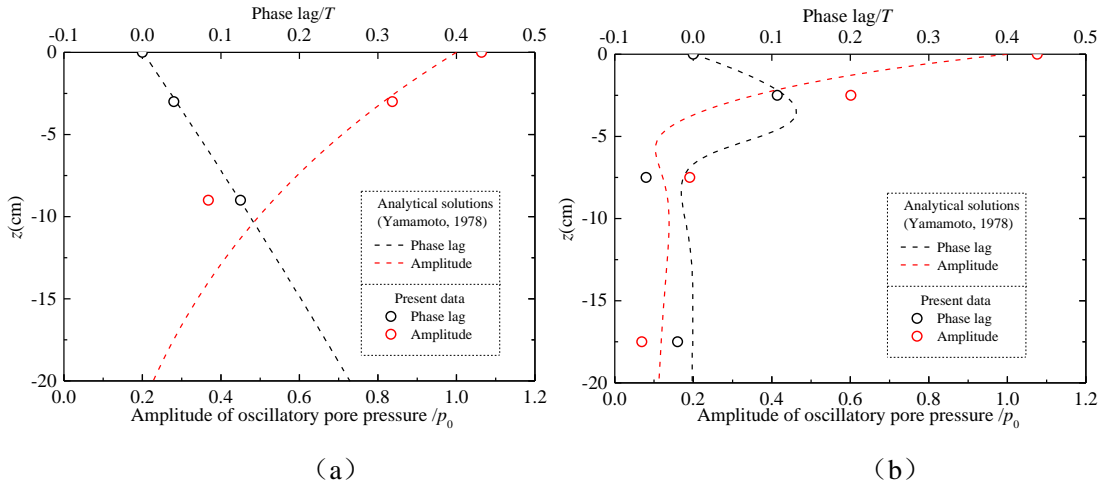


图 5 相位滞后与幅值衰减的试验值与理论解对比: (a) 砂土海床 (b) 粉土海床

Fig. 5 Comparisons of the vertical distributions of the excess pore pressure amplitude and phase-lag along the soil depth between experimental data and analytical solutions: (a) sandy seabed (b) silty seabed

3 结 论

本文基于理论分析与试验研究, 对砂土和粉土海床瞬态孔压响应的相位滞后与幅值衰减特性进行了探究, 主要得出了以下结论:

(1) 完全饱和与低饱和度海床内部瞬态孔压振荡幅值均呈现指数型衰减。对于完全饱和海床, 不存在相位滞后; 对于低饱和度海床, 推导了相位滞后的解析解。

(2) 海床的渗透系数与饱和度是控制相位滞后的关键参量, 渗透系数越小, 饱和度越低, 相位滞后在表层海床变化越剧烈。

(3) 砂土与粉土海床瞬态孔压响应的试验值与理论解吻合良好。砂土海床内部的相位滞后与幅值衰减变化梯度较小, 相位滞后随海床深度单调增加。粉土海床内部的相位滞后与幅值衰减变化梯度较大, 在表层海床, 相位滞后随海床深度呈先增大后减小的变化趋势; 在深层海床, 瞬态孔压响应较为微弱, 粉土海床内部的瞬态孔压响应特性与边界层类似。

致谢: 本研究得到国家杰出青年科学基金(编号: 11825205)及中国科学院战略性先导科技专项(B类)(编号: XDB22030202)资助。

参考文献

- 1 Miyamoto T., Yoshinaga S., Soga F., 1989. Seismic prospecting method applied to the detection of offshore breakwater units setting in the bed. Coastal Eng Jpn. 32, 103-112.
- 2 Christian J. T., Taylor P. K., Yen J. K. C., 1974. Large diameter underwater pipeline for nuclear power plant designed against soil liquefaction. The 6th Annual Offshore Technology Conference, Huston: Offshore Technology Conference, 597-606.
- 3 Zen, K., Yamazaki, H., 1990b. Oscillatory pore pressures and liquefaction in seabed induced by ocean waves. Soils Found. 30 (4), 147-161.
- 4 Seed H. B., Rahman M. S., 1978. Wave-induced pore pressure in relation to ocean floor stability of cohesionless soils. Mar Geotech. 3, 123-150.
- 5 Biot, M.A., 1941. General theory of three-dimensional consolidation. J. Appl. Phys. 26(2), 155-164.
- 6 Putnam, J.A., 1949. Loss of wave energy due to percolation in a permeable sea bottom. Trans. Am. Geophys. Union 30 (3), 349-356.
- 7 Moshagen, H., Torum, A., 1975. Wave induced pressures in permeable seabeds. J. Waterw. Harb. Coast. Eng. Div. 101 (1), 49-57.
- 8 Yamamoto, T., Koning, H.L., Sellmeijer, H., Hijum, E.V., 1978. On the response of a poro-elastic bed to water waves. J. Fluid Mech. 87 (01), 193-206.
- 9 Madsen, O.S., 1978. Wave-induced pore pressures and effective stresses in a porous bed. Geotechnique 28 (4), 377-393.
- 10 Hsu, J.R.C., Jeng, D.S., 1994. Wave-induced soil response in an unsaturated anisotropic seabed of finite thickness. Int. J. Numer. Anal. Meth.

GeoMech. 18 (11), 785–807.

11 Mei, C.C., Foda, M.A., 1981. Wave-induced responses in a fluid-filled poro-elastic solid with a free surface—a boundary layer theory. *Geophys. J. Int.* 66 (3), 597–631.

12 Mase, H., Sakai, T., Sakamoto, M., 1994. Wave-induced porewater pressures and effective stresses around breakwater. *Ocean Eng.* 21 (4), 361–379.

13 Cheng, L., Sumer, B.M., Fredsøe, J., 2001. Solution of pore pressure build up due to progressive waves. *Int. J. Numer. Anal. Meth. GeoMech.* 25, 885–907.

14 Higuera, P., Lara, J.L., Losada, I.J., 2014. Three-dimensional interaction of waves and porous coastal structures using OpenFOAM®. Part I: formulation and validation. *Coast. Eng.* 83, 243–258.

15 Sui, T.T., Zhang, C., Guo, Y.K., Zheng, J.H., Jeng, D.S., Zhang, J.S., Zhang, W., 2016. Three-dimensional numerical model for wave-induced seabed response around mono-pile. *Ships Offshore Struct.* 11, 667–678.

16 Zhang, C., Sui, T.T., Zheng, J.H., Xie, M.X., Nguyen, V.T., 2016. Modelling wave-induced 3D non-homogeneous seabed response. *Appl. Ocean Res.* 61, 101–114.

17 Tsui, Y.T., Helffrich, S.C., 1983. Wave-induced pore pressures in submerged sand layer. *Journal of Geotechnical Engineering, ASCE* 109 (4), 603–618.

18 Chang, S.C., Lin, J.G., Chien, L.K., Chiu, Y.F., 2007. An experimental study on non-linear progressive wave-induced dynamic stresses in seabed. *Ocean Eng.* 34 (17), 2311–2329.

19 Zhang, J.S., Li, Q.Z., Ding, C., Zheng, J.H., Zhang, T.T., 2016. Experimental investigation of wave-driven pore-water pressure and wave attenuation in a sandy seabed. *Adv. Mech. Eng.* 8 (6), 1–10.

20 Zhai, Y., Zhang, J., Jiang, L., Xie, Q., Chen, H., 2018. Experimental study of wave motion and pore pressure around a submerged impermeable breakwater in a sandy seabed. *Int. J. Offshore Polar Eng.* 28 (1), 87–95.

21 Qi, W.G., Li, C.F., Jeng, D.S., Gao, F.P., Liang, Z.D., 2018. Combined wave-current induced excess pore-pressure in a sandy seabed: Flume observations and comparisons with theoretical models. *Coastal Engineering* 147, 89–98.

22 Jeng, D.-S., 2018. Mechanics of Wave-Seabed-Structure Interactions: Modelling, Processes and Applications. Cambridge University Press, Cambridge.

23 Okusa, S., 1985. Wave-induced stress in unsaturated submarine sediments. *Geotechnique* 35 (4), 517–532.

24 Sakai, T., Hatanaka, K., Mase, H., 1992. Wave-induced effective stress in seabed and its instantaneous liquefaction. *Journal of Waterway, Port, Coastal and Ocean Engineering, ASCE* 118 (2), 202–206.

Wave-induced transient pore pressure in the sandy and silty seabeds: Phase-lag and amplitude-attenuation

Li Changfei^{1, 2}, Gao Fuping^{1, 2*}

¹(Key Laboratory for Mechanics in Fluid Solid Coupling Systems, Institute of Mechanics, Chinese Academy of Sciences,
Beijing 100190, China)

²(School of Engineering Science, University of Chinese Academy of Sciences, Beijing 100049, China)

Abstract: When water waves propagate over a porous seabed, transient pore pressures are induced, accomplished by phase-lag and amplitude-attenuation. Based on the analytical solution to Biot's consolidation equations for the response of a poro-elastic bed to water waves, an analytical solution of phase-lag for a partially saturated seabed is presented and then the key parameters for phase-lag are investigated. Theoretical study indicates that, the phase-lag gradient is significant with low permeability and low degree of saturation. In this study, the transient responses in a sandy and silty seabed were experimentally simulated with a flume. Transient pore pressure distributions in the flume observations are consistent with those of the analytical solutions for both sandy and silty seabed. In the surface layer of a silty seabed, the gradients of pore pressure amplitude and phase-lag are significant. Nevertheless, in a sandy seabed, the pore pressure gradients are lower than those in a silty seabed.

Key words: transient pore pressure, phase-lag, amplitude-attenuation, theoretical study, flume observation